

JGR Biogeosciences



RESEARCH ARTICLE

10.1029/2023JG007715

Key Points:

- Coastal hydrodynamics impose an important boundary condition on the production of N₂O in permeable sediments
- Less than 0.5% of seawater dissolved inorganic nitrogen is converted to N₂O due to forcing imposed by passing surface gravity waves
- Permeable sediments are a relatively minor source of N₂O emission in coastal waters of Port Phillip Bay

Supporting Information:

Supporting Information may be found in the online version of this article.

Correspondence to:

P. Cook, perran.cook@monash.edu

Citation:

Fowdar, H., Grant, S. B., Wong, W. W., Kessler, A., & Cook, P. (2024). Hydrodynamics control nitrous oxide production in eutrophic coastal permeable sediments. *Journal of Geophysical Research: Biogeosciences*, 129, e2023JG007715. https://doi.org/10.1029/2023JG007715

Received 18 JUL 2023 Accepted 13 JUN 2024

© 2024. The Author(s). This is an open access article under the terms of the Creative Commons Attribution License, which permits use, distribution and reproduction in any medium, provided the original work is properly cited.

Hydrodynamics Control Nitrous Oxide Production in Eutrophic Coastal Permeable Sediments

Harsha Fowdar¹, Stanley B. Grant^{2,3}, Wei Wen Wong¹, Adam Kessler⁴, and Perran Cook¹

¹Water Studies, School of Chemistry, Monash University, Melbourne, VIC, Australia, ²Occoquan Watershed Monitoring Laboratory, The Charles E. Via Jr Department of Civil and Environmental Engineering, Virginia Tech, Manassas, VA, USA, ³Center for Coastal Studies, Virginia Tech, Blacksburg, VA, USA, ⁴School of Earth, Atmosphere and Environment, Monash University, Melbourne, VIC, Australia

Abstract Permeable sediments, which make up almost half of the continental shelf worldwide, are potential sources of the important greenhouse gas N_2O from coastal regions. Yet, the extent to which interactions between these sediments and anthropogenic pollution produce N_2O is still unknown. Here we use laboratory experiments and modeling to explore the factors controlling N_2O production at a eutrophic site in a temperate shallow marine embayment (Port Phillip Bay, Australia). Our results show that denitrification is the main source of N_2O production within permeable sediments, but the extent to which N_2O is actually released is determined by the rate of seawater exchange with the sediment bed (which governs solute residence time within the bed). In wavedominated coastal areas, shallower water with more intense waves (*wave height* > 1 m) release the most N_2O , with up to 0.5% of dissolved inorganic nitrogen pumped into biologically active eutrophic sediment being released as N_2O . Our results suggest rates of N_2O production in coastal permeable sediments are generally low compared to other environments.

Plain Language Summary Permeable sands cover almost half of the coastal continental shelf around the world. The permeability of sand sediments, means water can flow through these sediments in complex patterns driven by waves and currents. This flow through the sediment can control nitrous oxide and methane production which are poorly understood. This is particularly important in regions impacted by nitrogen pollution where production of these greenhouse gases can be high. Here we combine experiments and modeling to explore the factors controlling N_2O production at a sandy site impacted by nitrogen pollution (Port Phillip Bay, Australia). Our results show the rate of nitrous oxide release to the water column is governed by the rate of seawater exchange with the bed. Shallower water with more intense waves (wave height exceeding 1 m) releases the most N_2O , with up to 0.5% of dissolved nitrogen pumped into the sediment being released as N_2O . Overall, these results suggest permeable sediments have relatively low rates of nitrous oxide release most of the time.

1. Introduction

Nitrous oxide, N_2O , is an important atmospheric greenhouse gas, contributing to climate change and stratospheric ozone depletion. Inland and coastal waters emit about 3% of global N_2O (0.6 Tg N (N_2O)/year⁻; 5^{th} IPCC assessment report–Ciais et al., 2013) while coastal areas account for approximately 15%–45% of the global oceanic N_2O source (Nevison et al., 2004). A more recent reconstruction of global oceanic N_2O source estimates an annual mean N_2O flux of 4.2 ± 1.0 Tg N/year (Yang et al., 2020) while Tian et al. (2020) studied global N_2O budget for 2007–2016 and found inland and coastal waters to emit 0.2 to 0.7 Tg N/year from anthropogenic sources (Tian et al., 2020). N_2O production in coastal areas is attributed to anthropogenic nitrogen inputs from a range of sources, including wastewater treatment plants, agricultural practices and groundwater (Seitzinger & Kroeze, 1998; Tian et al., 2020). Given that anthropogenic nitrogen inputs to estuarine and coastal ecosystems worldwide is increasing, an increase in future N_2O emissions from coastal areas is predicted (Bange, 2006). While N_2O production from terrestrial ecosystems and rivers and streams have been more extensively studied, there is a paucity of studies delving into the factors controlling production in coastal sediments.

 N_2O is produced as a by-product or intermediate of the biochemical processes of nitrification and denitrification respectively (Bange, 2006). In coastal environments, these processes can produce N_2O through interactions with sediments (O'Reilly et al., 2015). Permeable sediments comprise >40% of the continental margin worldwide (Riedl et al., 1972). Permeable sediments differ from fine-grained "impermeable" (or cohesive) sediments in that solute transport and exchange in permeable sediments are dominated by rapid advective flows as opposed to

FOWDAR ET AL. 1 of 14

Table 1Details of Flow Through Reactors Experiments (Experiment 1–3)

| Dimension and number of reactor (diameter × height) | Dissolved oxygen concentrations at the outlet (%sat) | Reactor pumping/flow rate (mL/min) | Concentration of substrate in inlet reservoir (µmol/L) |
|--|--|------------------------------------|--|
| Experiment 1: Effect of dissolved oxygen and NO ₃ ⁻ on N ₂ O production | | | |
| $4.8 \text{ cm} \times 1.0 \text{ cm} (n = 12)$ | ~0, 50, 100 | 0.1–10 | NO ₃ ⁻ (34, 80, 242, 840) |
| Experiment 2: Effect of ammonium concentrations on N ₂ O production | | | |
| $4.8 \text{ cm} \times 3 \text{ cm} (n = 9)$ | 60 ± 5 | 1.1–1.3 | NH ₄ ⁺ (5, 18, 36, 100, 358) |
| Experiment 3: N ₂ O consumption experiment | | | |
| $4.8 \text{ cm} \times 1.0 \text{ cm} (n = 12)$ | ~0 | 0.2–8 | N ₂ O (11–800) |

diffusion. It is thus strongly suspected that permeable sediments are hotspots of marine nitrogen cycling and its role needs to be better constrained (Chua et al., 2022; Huettel et al., 2014). As a result of their relatively high permeability and topography, small pressure gradients generated at the sediment-water interface (SWI) drive pore water flows through the sediment, thereby modulating spatial and temporal patterns of seawater circulation through these sediments (Huettel et al., 2014). Consequently, organic matter and other solutes from the water column transported into the seafloor contribute to oscillating oxic/anoxic conditions within these sediments. This can have a complex effect on redox processes such as the nitrogen cycle which is driven by oxic/anoxic transitions (Cardenas et al., 2008; Cook et al., 2006; Kessler et al., 2012, 2013; Precht et al., 2004). There is some evidence that permeable sediments are a potential source of N₂O (Jameson et al., 2021; Marchant et al., 2016; Schutte et al., 2015; Wong et al., 2021). However, the spatial and temporal variability of N₂O production caused by seawater recirculation through permeable sediments has been overlooked. It is still not fully known under what conditions (physical and/or biogeochemical), N₂O is more likely to be released from the sediment in coastal environments.

In coastal environments, surface gravity waves can drive the transport of material into and out of permeable sands (Fogaren et al., 2013; Hume et al., 2011; Precht & Huettel, 2004; Rodellas et al., 2020). Two forcing mechanisms contribute to this process: (a) wave pumping in which a passing surface water wave causes pressure at the SWI to oscillate in time, with higher and lower pressures under wave crests and troughs, respectively and; (b) flow- and topography-induced pressure gradients (or bedform pumping) where pore-water exchange occurs when orbital water motions in the wave boundary layer reach the seabed sediments. Undertaking gas flux measurements, whilst maintaining these exchange processes is difficult, and therefore coupled hydrodynamic/biogeochemical models in combination with bio-kinetic sediment rate constants provide a means to estimate sediment exchange rates and gain insights into the factors controlling this (Azizian et al., 2015; Kessler et al., 2012).

Here we combine wave data, bio-kinetic rate measurements of N_2O production in a novel Pumping and Streamline Segregation model (PASS, Azizian et al., 2015) to explore how the scale and rate of pore exchange govern the water residence time, nutrient cycling and N_2O production in seabed sediments. We focused specifically on the net N_2O produced by permeable sediments in Werribee, Port Phillip Bay, Australia. This eutrophic site is adjacent to a major sewage treatment plant which continuously discharges organic matter and inorganic nitrogen (Harris et al., 1996; Hirst et al., 2016). Rates of N_2O production estimated here therefore likely represent an upper range of emissions for this sediment type.

2. Methods

2.1. Laboratory Experiments

To investigate N_2O production pathways in permeable sediments and quantify corresponding kinetics, we performed laboratory manipulative experiments using flow through reactors (FTRs, as described by Evrard et al., 2013) on Werribee sediments (Table 1). In Experiment 1, we investigated N_2O production under oxicanoxic transitions (dissolved oxygen of inflow was varied from 267 to 109 to 0 μ mol/L N_2O 0 at four distinct N_2O 0 concentrations (34, 80, 242 and 840 μ mol/L). In Experiment 2, we investigated the effect of inflow N_2O 0 roduction under oxic conditions (152 μ mol/L N_2O 0). Experiment 2). These DIN concentrations were chosen based on the seasonal nutrient concentrations in Port

FOWDAR ET AL. 2 of 14

Phillip Bay (Wong et al., 2022). In Experiment 3, we measured the rate of N_2O consumption in permeable sediments at different water residence times.

Sediment cores and seawater were collected from the Werribee South beach. Intact sediment cores were collected using 50×4.1 cm (length \times inner diameter) acrylic cylinders and stoppered. Upon return to the laboratory, the top 5 cm of sediments from multiple cores were sliced and pooled to homogeneity before being sieved through a 2 mm mesh-size sieve to remove shell debris and large fauna to eliminate potential "void zones" or preferential flow paths as well as faunal death and decay during the experiment which would lead to unreliable kinetic measurements. It is possible this process can alter sediment biogeochemistry, however given that permeable sediments are regularly moved and disturbed this is generally not considered to lead to major alterations in process rates, and is standard practice in the field, for example, Marchant et al. (2016), Evrard et al. (2013). The sediment was packed separately into FTRs underwater to ensure no entrainment of air bubbles in the reactors. All the reactors were wrapped with aluminum foil to prevent light penetration and thus photosynthesis. For Experiment 1 and 2, filtered in situ bay water in separate reservoirs was purged continuously with either argon and/or air and was cycled through the sediment reactors. The reservoir for Experiment 3 was purged with 1,000 ppm N₂O gas. The reactors were left to stabilize overnight before the experiments were started. The size of the reactors used, the dissolved oxygen conditions of the reservoirs and the flow rate of the circulated bay water were adjusted based on different experiments as outlined in Table 1. The dissolved oxygen (DO) in the reservoir and the outlet of the reactor was constantly measured with a DO probe (Hach HQ40d) and an optical flow through-cell sensor (Firesting Oxygen meter, Pyroscience), respectively. Approximately an hour after the experimental conditions were established, porewater samples were collected from the outlet of each reactor using gastight glass syringes. Samples were transferred to separate 12.5 mL gas-tight exetainers (filled to overflowing) and preserved with 25 μL HgCl₂ for the analysis of N₂O gas. Approximately 10 mL of sample from each reactor was also collected and filtered through 0.2 μm pore-size filter for the analysis of NO₃⁻, NO₂⁻, and NH₄⁺ concentrations. Similarly, samples were also collected from the reservoirs when adjusted with different dissolved oxygen and nutrient concentrations. The N₂O samples were stored at room temperature while nutrients samples were stored frozen until analysis. The concentrations of NOx (NO₃⁻+NO₂⁻), NO₂⁻ and NH₄⁺ were determined spectrophotometrically on a Lachat Quickchem 8000 following the procedures in Standard Methods for Water and Wastewater (APHA, 2005). N₂O concentrations in the headspace were determined using a VICI Trace Gas Analyzer. Prior to the gas measurement, $6\,\text{mL}$ of headspace was introduced by replacing $6\,\text{mL}$ of water with helium. The final N₂O concentration in the water samples was corrected and calculated according to Weiss and Price (1980).

2.2. Mechanistic Modeling Approach

Our simulations build upon the model Pumping and Streamline Segregation Model (PASS; Azizian et al., 2015), which takes into account advective pumping and biocatalytic transformation of dissolved inorganic nitrogen within sediment beds. In the following, we briefly describe the model, its validation and steps for data processing and synthesis used to model fluxes across the SWI in coastal settings.

2.2.1. General Approach: Hydrodynamic Conditions

Hydrodynamic (wave) parameters for Werribee, Port Phillip Bay were obtained from https://vicwaves.com.au/ (this data set is part of a study measuring sea climate along Victoria's coasts as part of the Victorian Coastal Monitoring Program). We used data from 1 January 2021 to 30 August 2022 (20 months of time series wave data), containing significant wave height and mean wave period, measured by wave buoys at a water depth of 12 m. Wavelength, L_w was calculated using the dispersion equation:

$$L_{w} = \frac{gT^{2}}{2\pi} \times \tanh\left(\frac{2\pi d}{L_{w}}\right) \tag{1}$$

where T represents the wave period, g is gravity and d is the water depth.

We analyzed variation in pore water exchange and N_2O production spatially with distance from shore, namely at water depths of 12 m (as above) and 2 m. Measured wave heights, H_w at a water depth of 12 m were translated to corresponding heights at 2 m water depth using the shoaling coefficient equation (Ippen, 1966) as follows:

FOWDAR ET AL. 3 of 14

1698961, 2024, 7, Downloaded from https://agupubs.onlinelibrary.wiley.com/doi/10.1029/2023JG007715, Wiley Online Library on [21/07/2024]. See the Terms and Co

$$k_s = \frac{H}{H_o} = \left(\tanh(k \times d) \times \left(1 + \left(\frac{2kd}{\sinh(2kd)}\right)\right)\right)^{-0.5}$$
 (2)

where k = wave number = $2\pi/L_w$, H_o is wave height in deep water and H is that at 2 m depth.

In order to understand the effect of wave conditions on the efflux of N_2O , we grouped wave events according to their H_w : (a) Category 1 (calm conditions), $H_w < 0.1$ –0.5 m, representing background conditions; (b) Category 2 (moderate conditions) H_w 0.5–1.0 m, that is, above background conditions and (c) Category 3 (significant conditions) with $H_w > 1$ m. Average wave parameters from each event were used in the subsequent pore water exchange and efflux calculations (Sections 2.2.2 and 2.2.3). The driving pore water exchange mechanism was determined based on the d/L_w ratio of each wave event, with wave pumping prevalent at $\frac{1}{2} < d/L_w < 1$ and bedform pumping at $d/L_w < \frac{1}{2}$ as per Precht and Huettel (2003).

2.2.2. Pore Water Exchange and Transit Time

The seawater exchange modeling combines previously published physics-based models for bedform pumping (Azizian et al., 2015; Elliott & Brooks, 1997) and wave pumping (King et al., 2009; Russoniello et al., 2018). Porewater exchange due to bedform pumping is driven by pressure variation at the SWI arising from the acceleration and deceleration of flow over the bedform and boundary layer separation effects.

An idealized model of this process, first introduced by Elliott and Brooks (1997) (see also Grant et al. (2014)), yields the following formula for the maximum Darcy flux of water across the SWI induced by bedform pumping:

$$q^{EB} = \frac{2\pi h_m^{EB} k_h}{\lambda} \tag{3}$$

where h_m^{EB} is the amplitude of the flow-induced pressure head variation across the bedforms, k_h is the sediment hydraulic conductivity, λ represents the bedform (or ripple) wavelength. The amplitude of the pressure head variation, h_m^{EB} , can be estimated as $(0.28 \ U_w^2/2 \ g) \ (\Delta/0.34)^{\gamma}$ (Elliot & Brooks, 1997; Grant et al., 2020) where the variables U_w represent the average steady-unidirectional flow velocity, g is the gravitational acceleration constant, $\Delta = \eta_r/d$, η_r is the ripple height, and d is the water depth. The empirical exponent, γ is taken as 3/8 (if $\Delta < 0.34$) or 3/2 (if $\Delta > 0.34$). Here we assume that the magnitude of the exchange flux due to unidirectional flow is comparable to the exchange flux induced by surface-wave driven oscillatory flow (as per Precht & Huettel, 2003).

Porewater exchange due to wave pumping is driven by the time varying hydrostatic pressure beneath passing surface waves. Small amplitude wave theory predicts that the pressure head at the SWI induced by the propagation of a single harmonic surface wave can be written as: $h(x,t) = aK_p \sin(kx - \sigma t)$, where the variables represent time t, the horizontal distance along the bed x, pressure response factor $K_p = 1/\cosh(kd)$, the depth of the water column d, the surface wave's amplitude a, wave number $k = 2\pi/L_w$, and angular frequency $\sigma = 2\pi/T$. This solution implies that the pressure head at the bed induced by a traveling surface wave propagates in the positive x-direction at celerity $c = \sigma/k = L_w/T$. We define a new coordinate system following the pressure wave: $x' = x - \sigma t/k$. Expressed in terms of this new coordinate system, $h(x', t) = h_m \sin(kx')$ where the variable $h_m = aK_p$ is the maximum pressure head amplitude induced by the surface wave. This equation is isomorphic to the sinusoidal pressure head applied to a flat SWI in the classic bedform pumping model first introduced by Elliott and Brooks (1997) and mentioned above. Thus, their analytical solution for the two-dimensional interstitial velocity field can be applied directly to our problem. The resulting maximum Darcy flux across the SWI due to wave pumping is:

$$q^{SW} = \frac{2\pi h_m^{SW} k_h}{L_w} \tag{4}$$

The age of water exiting the sediment bed and returning to the overlying water column—or transit time distribution—takes into account the age of water parcels transiting along individual streamlines through the sediment

FOWDAR ET AL. 4 of 14

1698961, 2024, 7, Downloaded from https://agupubs.onlinelibrary.wiley.com/doi/10.1029/2023JG007715, Wiley Online Library on [21/07/2024]. See the Terms

2.2.3. PASS Benthic Fluxes

PASS combines the flow field for advective pumping (bedform or wave) with biogeochemical reactions for aerobic respiration (AR), nitrification (NI), denitrification (DN) and ammonification (AM) (Azizian et al., 2015). PASS neglects solute transport through the sediment by molecular diffusion and mechanical dispersion and assumes that the sediment is homogeneous and infinitely deep; a previous study by Grant et al. (2014) specifically examined the relative importance of diffusion, mechanical dispersion, and advection on solute transport through bedforms by bedform pumping and found that, for most environmentally relevant conditions, advection dominates. The PASS model has also been validated with laboratory measurements of nitrogen transport and transformation in ripples under hydrodynamic conditions similar to those found in coastal settings (Azizian et al., 2015). We added the kinetics for N_2 O production into the existing PASS model; specifically, the rate of N_2 O production was modeled as a function of the rates of nitrification R_{NJ} and denitrification R_{DN} as follows:

$$R_{N,O} = f_{dn}R_{DN} + f_{ni}R_{NI}; \tau < \tau_{crit}, C_{NO_{-}} > 0$$
(5)

where f_{dn} and f_{ni} are denitrification and nitrification fractions respectively, calibrated to experimental data. While N₂O accumulates in the presence of nitrate, this is followed by a net consumption when oxidized nitrogen become limiting (Marchant et al., 2016). To account for N₂O consumption, N₂O concentration along a streamline was taken to be zero upon reaching a certain threshold transit time (Reeder et al., 2018). The threshold transit time (τ_{crit}) was taken to be 6 hr. This constituted our Model A. Based on results of Experiment 3, complete N₂O consumption was observed at a transit time of 20 min. Sensitivity analysis performed with τ_{crit} = 20 min showed agreement with results of Model A (Figure S3 in Supporting Information S1, Werribee data set, Model A.1).

Based on additional flow through reactor experiments with varying NH_4^+ concentrations (Experiment 2), we developed Model B where N_2O production from nitrification and denitrification was simulated separately. N_2O production due to denitrification was modeled as above (i.e., N_2O net production at $\tau < \tau_{crit}$, and complete consumption at $\tau > \tau_{crit}$). For N_2O production due to nitrification, a reduced value of f_{ni} (Text S1 and Table S1 in Supporting Information S1) was adopted which accounted for net production (i.e., production—consumption) for all τ . As modeled fluxes between the two models were comparable (their ratio approached unity for the most important wave climates; Figure S4 in Supporting Information S1), results for Model A only are reported.

Monod rate expressions were adopted for the rates of aerobic respiration R_{AR} , ammonification R_{AM} , nitrification R_{NN} , and denitrification R_{DN} all in units of mol/m³/s:

$$R_{AR} = \frac{R_{min}C_{O_2}}{C_{O_2} + K_{O_2}^{sat}} \tag{6}$$

$$R_{AM} = \frac{1}{\gamma_{CN}} R_{AR} \tag{7}$$

$$R_{NI} = k_{Ni} C_{O_2} C_{NH^+} \tag{8}$$

$$R_{DN} = \theta_{O_2}^{inh} \kappa \frac{R_{min} C_{NO_3^-}}{C_{NO_3^-} + K_{NO_3^-}^{sat}}; \theta_{O_2}^{inh} = \frac{K_{O_2}^{inh}}{C_{O_2} + K_{O_3}^{inh}}$$
(9)

where R_{min} is the respiration rate of sediment organic matter in mol/m³/s, γ_{CN} is a constant for ammonification, k_{Ni} is a bimolecular nitrification rate constant in m³/mol/s, $K_{O_2}^{sat}$ and $K_{NO_3}^{sat}$ are half-saturation constants for aerobic respiration and denitrification respectively in mol/m³, C_{O_2} , $C_{NH_4^+}$, $C_{NO_3^-}$ are the concentrations of oxygen, ammonium and nitrate respectively in mol/m³, $K_{O_2}^{inh}$ is the half saturation constant for O_2 inhibition of denitrification in mol/m³ and κ is an empirical factor, taken as 0.05. Anammox was neglected because previous studies

FOWDAR ET AL. 5 of 14

agupubs on linelibrary wiley com/doi/10.1029/2023JG007715, Wiley Online Library on [21/07/2024]. See the Terms/

have found it to be a minor contribution to nitrogen cycling in coastal permeable sediments (e.g., Evrard et al., 2013).

The concentrations of oxygen (C_{O_2}) , ammonium $(C_{NH_4^+})$ and nitrate $(C_{NO_3^-})$ along any streamline through the sediment evolve with water parcel age (τ) according to the following set of mass balance expressions:

$$\frac{dC_{O_2}}{d\tau} = -R_{AR} - 2R_{NI} \tag{10}$$

$$\frac{dC_{NO_3^-}}{d\tau} = R_{NI} - R_{DN} \tag{11}$$

$$\frac{dC_{NH_4^+}}{d\tau} = R_{AM} - R_{NI} \tag{12}$$

the benthic flux of the *i*th species (incl. nitrous oxide), U_i was calculated as follows (Azizian et al., 2015):

$$U_i = -k_m [C_i(0) - C_{i,bed}] (13a)$$

$$C_{i,bed} = \int_{-\infty}^{\infty} C_i \left(\overline{\tau_R} = \mathbf{D} \mathbf{a} \overline{\tau_f}; chemistry \right) \frac{dF_{RTD}}{d \log_{10} \overline{\tau_f}} d \log_{10} \overline{\tau_f}$$
 (13b)

 $C_i(0)$ represents the concentration of the *i*th species in seawater entering the sediment bed in the downwelling zone, $C_{i,bed}$ represents the flow-weighted concentration of the *i*th species leaving the sediment bed in the upwelling zone, and k_m is the average volume of water flowing across the SWI per unit area of bed surface (i.e., the average Darcy flux across the SWI also sometimes called the pore water flushing rate). The average Darcy flux is related to the maximum Darcy fluxes indicated above for bedform and wave pumping (see Equations 3 and 4) by $k_m = q$. The Damköhler number (\mathbf{Da}) represents the ratio of time scales for transport (τ_T) and respiration of sediment organic matter ($\tau_R = k_{O_2}^{sat}/R_{min}$). To determine biogeochemical pathways dominating N₂O production, we evaluated the contribution of each nitrogen source to the efflux of N_2O as per Azizian et al. (2015).

2.2.4. Hydraulic and Biogeochemical Variables Adopted for the Simulations

Sediment permeability of 1.01×10^{-11} m², previously measured in Port Phillip Bay (Evrard et al., 2013), was adopted for the simulation. Bedform or ripple geometry: the ripple length, λ_r was taken to be 0.4 m, which is close to the average of 0.5 m in coastal environments, Shum (1993). The ripple height, η_r was estimated based on the empirical equation by Warner et al. (2008) for ripples formed in wave-dominated environments.

$$\frac{\eta_r}{\lambda_r} = \exp\left[-0.095 \left(\ln \frac{d_o}{\eta_r} \right)^2 + 0.442 \ln \frac{d_o}{\eta_r} - 2.28 \right]$$
 (14)

for $d_o/\eta_r > 10$; if $d_o/\eta_r \le 10$, $\eta_r/\lambda_r = 0.17$. Variable d_o represent the diameter of the orbital motion. d_o was calculated as per linear potential flow theory (Wiberg & Harris, 1994) as follows:

$$d_o = \frac{H_w}{\sinh(kd)} \tag{15}$$

Near-bed wave velocity, U_w at a depth of 12 m was estimated using the empirical relationship given by Fogaren et al. (2013): $U_w = 0.19*H_w + 0.054$. For shallower depths (i.e. 2 m), U_w was estimated from the relationship given by linear wave theory (Wiberg & Harris, 1994) as follows:

$$u_w = \frac{\pi d_o}{T} \tag{16}$$

FOWDAR ET AL. 6 of 14

Biogeochemical parameters (Table S2 in Supporting Information S1) were either obtained from the literature or calibrated to experimental data. Details of the calibration exercise are provided Text S2 in Supporting Information S1.

2.2.5. Validation With Numerical Model, COMSOL

We compared PASS results (wave pumping) with numerical simulations performed using the finite element model COMSOL (Bardini et al., 2012; Grant et al., 2014). For each wave condition, the two-dimensional domain was L m wide and $3 \times L$ m thick and the number of elements ranged from approx. 180,000 to 235,000, with most clustered around the SWI. The pressure distribution over the sediment bed, identical to the analytical pressure equation (as above), was applied as a top boundary condition to predict benthic fluxes. In addition, the following boundary conditions were imposed: (a) constant concentration at the top boundary; (b) a no-flux condition at the bottom boundary and (c) periodic boundaries at the edges. Parameter values followed those in Grant et al. (2014) and those adopted in PASS. The rate equations in the reactive transport model (Bardini et al., 2012) were as per above. We performed seven simulations (run to steady-state), encompassing a range of wave conditions (Table S3 in Supporting Information S1). The agreement in benthic fluxes between the two models is highest (within roughly 5%–15%) when pore exchange rates are highest and decreases as the exchange rate decreases. PASS has been previously validated with COMSOL with respect to benthic flux estimation as a result of bedform pumping as per Azizian et al. (2015).

2.3. Sensitivity and Statistical Analysis

In order to determine the most influential physical and chemical factors governing pore water exchange and N_2O efflux we conducted a global Monte Carlo sensitivity analysis of possible model parameter combinations as compiled from the literature (Table S4 in Supporting Information S1). A uniform distribution bounded by the literature values was created for each parameter (12 in total). We generated 10,000 Monte Carlo simulations where each simulation involves randomly sampling and recording a set of parameters from their uniform distributions and estimating the pore water exchange and N_2O efflux in each wave category at the two water depths. Then we used statistical inference tools to identify the key drivers of N_2O production at different spatial and temporal scales. In the first instance, we computed the Spearman Rank correlation between each metric and the pore water exchange rate and N_2O efflux to screen out the most influential physical and biochemical parameters at each water depth and for each wave category. Then we applied a multiple regression model to evaluate percent variance explained and relative importance of each metric to N_2O efflux in coastal permeable sediments:

$$\ln(N_2O \text{ efflux}) = \beta_0 + \beta_1 \ln(H_w) + \beta_2 \ln(k_h) + \beta_3 \ln(H_b) + \beta_4 \ln(\text{Cno3in}) + \beta_5 \ln(\text{Cnh3in}) + \beta_6 \ln(f_{ni})$$

$$+ \beta_7 \ln(f_{dn}) + \beta_8 \ln(\text{rmin}) + \beta_9 \ln(\text{kni}) + \varepsilon$$
(17)

where H_w is wave height, k_h is sediment hydraulic conductivity, H_b is ripple height, Cno3in is nitrate concentration in overlying seawater, Cnh3in is ammonium concentration in overlying seawater, f_{ni} is nitrification associated emission fraction, f_{dn} denitrification associated emission fraction, rmin is sediment respiration rate, kni is nitrification bi molecular constant, the β s are the regression coefficients and ε is random error. We applied an analysis of variance to nested models to quantify the sum of squares and hence percent variance explained by each metric.

Further, to test the hypothesis that N_2O efflux produced as a result of bedform-driven pore water exchange is significantly higher than wave-driven exchange, we conducted a Kolmogorov-Smirnov test on model outputs.

The dimensionless flux of N_2O , $F*N_2O$ was calculated as the ratio between N_2O efflux and the total flux per unit bed area of dissolved inorganic nitrogen species (NO_3 and NH_4) in seawater entering the sediment ($FDIN_0$) (following Marzadri et al., 2017). The theoretical N_2O yield was calculated as the ratio of N_2O efflux and total denitrification fluxes.

FOWDAR ET AL. 7 of 14

21698961, 2024, 7, Downloaded from https://agupubs.onlinelibrary.wiley.com/doi/10.1029/2023JG007715, Wiley Online Library on [21/07/2024]. See the Terms and Conditions

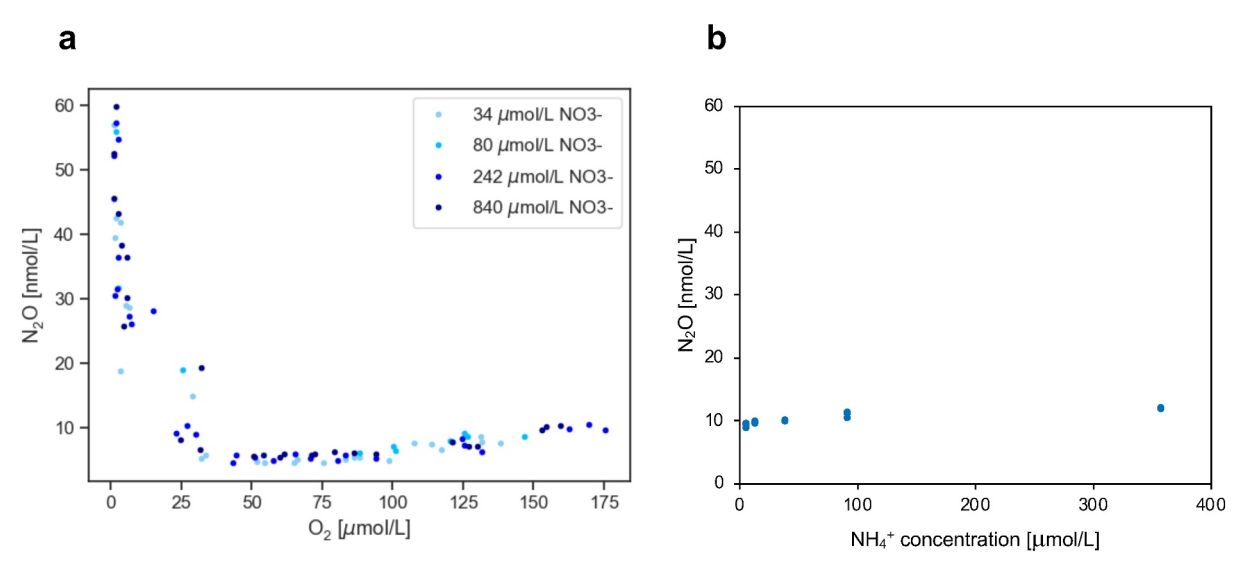


Figure 1. Ex situ measurements of N_2O dynamics in permeable sediments, Werribee, Port Phillip Bay (a) flow through reactor (FTR) measurements of N_2O production during anoxic-oxic transition across different NO_3^- levels (34, 80, 242, 840) in μ mol/L. (b) FTR measurements of N_2O production under oxic conditions (153 μ mol/L O_2) across different NH_4^+ levels. All measured points shown.

3. Results and Discussion

3.1. N₂O Production in Permeable Sediments

 N_2O production under anoxic-oxic transitions and varying NO_3^- levels is shown in Figure 1a. Irrespective of inflow NO_3^- , N_2O production peaked during low O_2 , and decreased sharply with increased O_2 , indicating production during anoxic denitrification; this was equivalent to an N_2O production rate of 1.3% of the modeled rate of denitrification. N_2O increased to a small degree at >1 μ mol/L O_2 , likely from nitrification, the rate of which was equal to 1.2% of the modeled nitrification rate. N_2O production was found to be insensitive to NH_4 concentrations under oxic conditions (Figure 1b); N_2O was consistently produced at a concentration of approximately 10 μ mol/L, the rate of which corresponded to 0.023%, on average, of the measured rate of nitrification. Results of the rate of N_2O consumption at different water residence times can be found in Supplementary Information. These fractions are similar to previously reported N_2O emissions for rivers, reservoirs and estuaries (Maavara et al., 2019).

When rate kinetics were coupled with coastal hydrodynamics (i.e., wave climate data), F^*N_2O ranged from 0.00018%–0.48% (average of 0.064%) at a depth of 2 m under DIN concentrations of 17.5 μ mol/L NH₄⁺ and 51 μ mol/L NO₃⁻ (which are within the concentrations previously measured in Werribee, Wong et al., 2022). F^*N_2O values for 95% of the simulations were lower than the IPCC proposed emission factor (EF) of 0.26% (IPCC, 2019) and 46% of the simulations were within the global EFs estimates for rivers, estuaries, and reservoirs of 0.025%–0.16% by Maavara et al. (2019). While EFs in these studies refer to N₂O emissions as a function of DIN concentrations/denitrification/nitrification, our F^*N_2O estimates refer to net N₂O produced by the sediments relative to total DIN flushed through the sediment; hence, N₂O emissions from coastal permeable sediments are likely to be lower than our F^*N_2O estimates.

Denitrification of seawater NO_3^- accounted for approximately 88% of sedimentary N_2O production. This is consistent with the literature which suggest denitrification dominates N_2O production compared to nitrification (Marchant et al., 2018; Seitzinger, 1988). Modeled denitrification rates of the sediments $(1,872 \ \mu mol/m^3/h$ average) were, on average, an order of magnitude higher than modeled nitrification rates $(126 \ \mu mol/m^3/h$ average) which could explain the dominance of denitrification in N_2O generation. The corresponding N_2O yield (i.e., ratio of N_2O/N_2) ranged between <0.01% and 1.8% (average of 0.17%). These are within the range previously observed in streams (Beaulieu et al., 2011), lake, river and coastal marine sediments (Seitzinger, 1988) of 0.1%–6% with the highest ratios typically observed in highly polluted sediments.

FOWDAR ET AL. 8 of 14

21698961, 2024, 7, Downloaded from https://agupubs.onlinelibrary.wiley.com/doi/10.1029/2023JG007715, Wiley Online Library on [21/07/2024]. See the Terms and Conditions (https://agupubs.on/doi/10.1029/2023JG007715, Wiley Online Library on [21/07/2024].

3.2. Temporal and Spatial Variability in Exchange Rate and N2O

We compared N_2O production across different wave climates in relatively shallow (2 m) and deep (12 m) waters at Werribee. Calm waves (<0.1–0.5 m H_w) occurred 73% of the time, moderate waves (0.5–1.0 m H_w) 23% of the time and significant waves (>1.0 m H_w) 4% of the time. In shallow water (2 m), pore water exchange is overwhelmingly controlled by bedforms (Figure 2a). In deep water (12 m), wave pumping contributes to 100% of pore water exchange for moderate waves and 85% for significant waves (Figure 2b). Simulated pore-water exchange rates were comparable to the literature (Mu et al., 1999; Precht & Huettel, 2003; Riedl et al., 1972; Russoniello et al., 2018), ranging from 1 to 330 L/m²/d for depths of 2–12 m. According to Precht and Huettel (2003), 50–100 L/m²/d is a moderate value for advective pore water exchange in permeable shelf sediment exposed to oscillating flow near the sediment bed.

Furthermore, exchange rates varied by a factor of 17 on average between calm and the most significant waves (2 m water; Figure 2a). Exchange rates decreased by approximately five times in 12 m water under the most significant waves. Paralleling pore water exchange rates, N_2O production rates also increased with increasing wave height. $F*N_2O$ increased by two orders of magnitude, on average, from the calm to the most intense waves in 2 m waters (Figure 2c) and decreased by up to four orders of magnitude from 2 to 12 m deep waters. N_2O efflux tended to follow the same pattern as $F*N_2O$, with a corresponding increase in N_2O efflux of up to five orders of magnitude from calm to the most intense waves (Figure 2e; Figure S2a in Supporting Information S1). Predicted N_2O efflux were relatively low (mostly <5 μ mol/m²/d) during calm waves at Werribee. Calmer waves are characterized with longer residence times (Figure S5 in Supporting Information S1), and consequently lower N_2O production rates. N_2O efflux decreased by several orders of magnitude in deep (12 m) relative to shallow (2 m) waters (Figure S2 in Supporting Information S1). N_2O efflux produced by bedform-driven pore water exchange significantly exceed those produced by wave-driven pore water exchange (p < 0.01) due to their shorter residence times (Figure S5 in Supporting Information S1) which could be one of the reasons behind the difference in the degree of N_2O production across water depths.

Based on the seasonal variability in nutrient loading in Port Phillip Bay (Wong et al., 2022) and DIN-dependence of N_2O production (e.g., Murray et al., 2015; Turner et al., 2016), we evaluated how N_2O efflux in Werribee responds to varying NO_3^- and NH_4^+ concentrations in the water column within the range previously measured in surface waters in Port Phillip Bay. Model predicted N_2O efflux increased by approximately three-fold, on average, in the presence of high NH_4^+ (358 μ mol/L) and high NO_3^- (315 μ mol/L), with the highest increase in the presence of high intensity waves (Figure S2a in Supporting Information S1). On the other hand, N_2O efflux remained low under the range of studied DIN_O at a depth of 12 m (<1 μ mol/m²/d; Figure S2b in Supporting Information S1). Similar trends in DIN concentrations and wave conditions were found for F*N₂O (Figures 2e and 2f). In the presence of high seawater NH_4^+ , denitrification contributed approximately 40% followed by coupled nitrification-denitrification and nitrification (28% each) while at high seawater NO_3^- , most of the N_2O produced was derived from denitrification (>95%). Given that $F*N_2O$ slightly decreased with increase in DIN concentrations, the higher N_2O efflux can be attributed to a higher mass of NH_4^+ and NO_3^- being flushed across the SWI. Although oxygen is known as a key variable controlling N_2O fluxes, bottom water O_2 concentration was held constant at 250 μ mol/L as we expected this to be close to saturation at the margins of this well mixed system.

3.3. Factors Regulating N₂O Fluxes in Wave-Driven Environments

In our Monte Carlo simulation, $F*N_2O$ (and hence N_2O efflux) was found to not depend on pore water exchange alone but also on biogeochemical factors. In shallower waters (2 m), the magnitude of the pore water exchange mostly dictates the corresponding magnitude of N_2O efflux, with wave height explaining 79% of the variability. Other factors including emission factors, DIN concentrations, sediment permeability and ripple geometry only explained a further 6% of the variance in N_2O efflux at a depth of 2 m. There are some differences between wave conditions (i.e., H_w). Biogeochemical factors become more important in influencing N_2O production during the most intense wave events compared to calm and moderate waves. For instance, during the most intense wave conditions, the emission fractions and seawater NH_4^+ concentrations explain 42% and 32% of the variability in N_2O efflux respectively. DIN_O can exert a substantial influence on N_2O efflux. For instance, at a depth of 2 m, average N_2O efflux decreased by 16%, 14% and 10% under calm, moderate and significant wave conditions during the sensitivity analysis when DIN_O was fixed to typical NO_3^- and NH_4^+ concentrations compared to when DIN_O were varied. In deeper waters (12 m), both the pore water exchange rate and N_2O production in the

FOWDAR ET AL. 9 of 14

21698961, 2024, 7, Downloaded from https://agupubs.onlinelibary.wiley.com/doi/10.1029/2023JG007715, Wiley Online Library on [21/07/2024]. See the Terms and Conditions (https://onlinelibrary.wiley.com/doi/10.1029/2023JG007715, Wiley Online Library on [21/07/2024]. See the Terms and Conditions (https://onlinelibrary.wiley.com/doi/10.1029/2023JG007715, Wiley Online Library on [21/07/2024]. See the Terms and Conditions (https://onlinelibrary.wiley.com/doi/10.1029/2023JG007715, Wiley Online Library on [21/07/2024]. See the Terms and Conditions (https://onlinelibrary.wiley.com/doi/10.1029/2023JG007715, Wiley Online Library on [21/07/2024]. See the Terms and Conditions (https://onlinelibrary.wiley.com/doi/10.1029/2023JG007715, Wiley Online Library on [21/07/2024]. See the Terms and Conditions (https://onlinelibrary.wiley.com/doi/10.1029/2023JG007715, Wiley Online Library on [21/07/2024]. See the Terms and Conditions (https://onlinelibrary.wiley.com/doi/10.1029/2023JG007715, Wiley Online Library on [21/07/2024]. See the Terms and Conditions (https://onlinelibrary.wiley.com/doi/10.1029/2023JG007715, Wiley Online Library on [21/07/2024]. See the Terms and Conditions (https://onlinelibrary.wiley.com/doi/10.1029/2023JG007715, Wiley Online Library on [21/07/2024]. See the Terms and Conditions (https://onlinelibrary.wiley.com/doi/10.1029/2023JG007715, Wiley Online Library on [21/07/2024]. See the Terms and Conditions (https://onlinelibrary.wiley.com/doi/10.1029/2023JG007715, Wiley Online Library on [21/07/2024]. See the Terms and Conditions (https://onlinelibrary.wiley.com/doi/10.1029/2023JG007715, Wiley Online Library on [21/07/2024]. See the Terms and Conditions (https://onlinelibrary.wiley.com/doi/10.1029/2023JG007715, Wiley Online Library on [21/07/2024]. See the Terms and Conditions (https://onlinelibrary.wiley.com/doi/10.1029/2023JG007715, Wiley Online Library.wiley.com/doi/10.1029/2023JG007715, Wiley Online Library.wiley.com/doi/10.1029/2023JG007715, Wiley Online Library.wiley.com/doi/10.1029/2023JG007715, Wiley Onlin

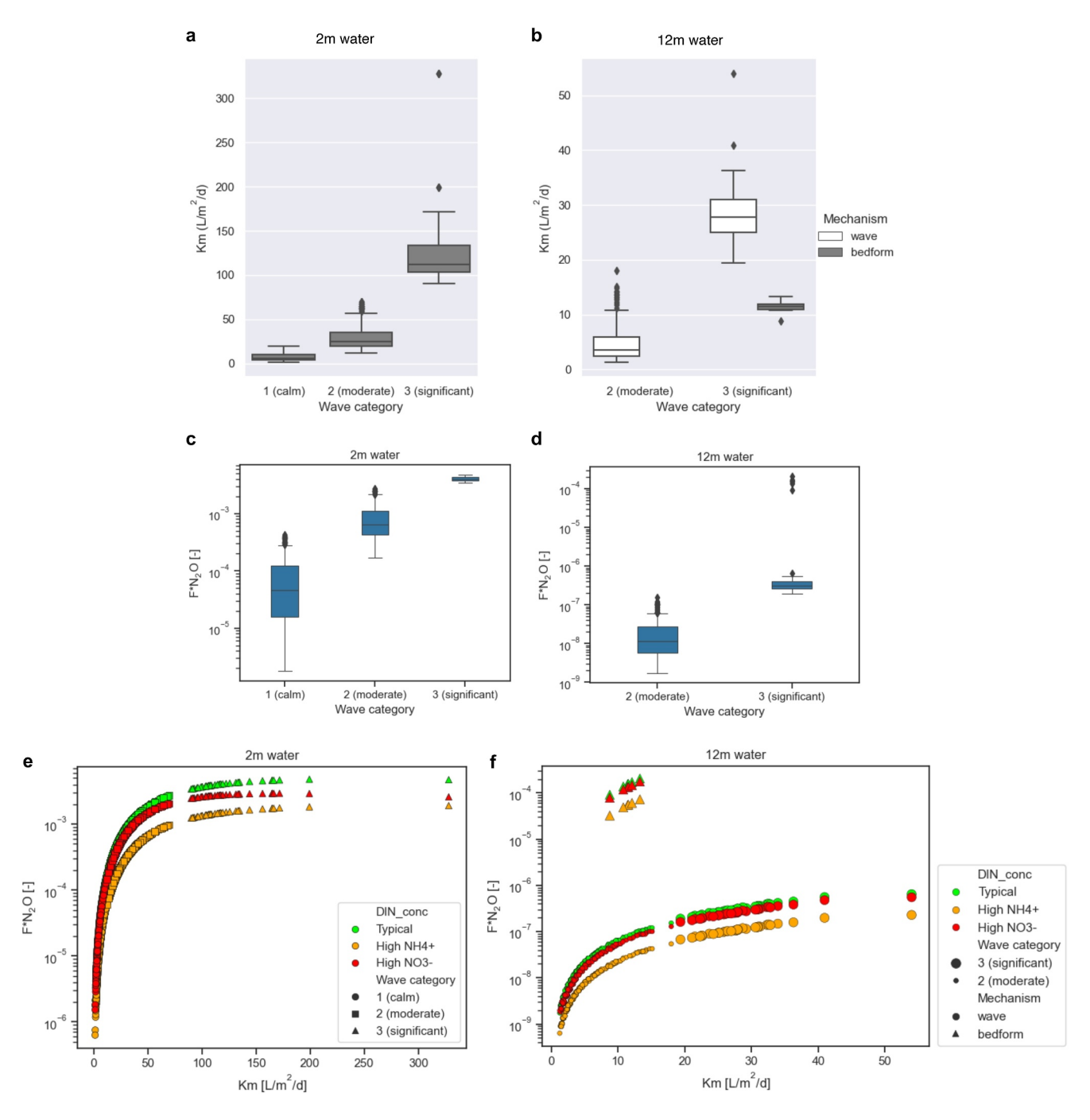


Figure 2. Simulated pore-water exchange rates and N_2O produced in sediment beds in 2 and 12 m water in Werribee, Port Phillip Bay. Calm conditions (<0.1–0.5 m H_w) occurred 73% of the time, moderate conditions (0.5–1.0 m H_w) 23% and significant wave conditions (>1.0 m H_w) occurred 4% of the time. Pore-water exchange is driven by two types of mechanisms, namely wave pumping and bedform (interaction of flow with bottom topography) pumping. (a) Exchange rates in 2 m water; (b) Exchange rates in 12 m water; (c) $F*N_2O$, net N_2O production within permeable sediments in 2 m water; (d) $F*N_2O$, net N_2O production within permeable sediments in 12 m water; (e) Relative variation of $F*N_2O$ with pore-water exchange in 2 m water; (f) Relative variation of $F*N_2O$ with pore-water exchange in 12 m water. The different symbols correspond to the different wave conditions experienced over the period 1 January 2021 to 30 August 2022. The different colors correspond to different inflow DIN concentrations in the water column, whereby typical = 17.5 μmol/L NH_4^+ and 51 μmol/L NO_3^- ; High $NH_3 = 358$ μmol/L NH_4^+ and 51 μmol/L NO_3^- and High $NO_3^- = 17.5$ μmol/L NH_4^+ and 315 μmol/L NO_3^- . These concentrations are within the range of values previously measured in Werribee, Port Phillip Bay (Wong et al., 2022).

FOWDAR ET AL. 10 of 14

21698961, 2024, 7, Downloaded from https://agupubs.onlinelibary.wiley.com/doi/10.1029/2023JG007715, Wiley Online Library on [21/07/2024]. See the Terms and Conditions (https://onlinelibrary.wiley.com/doi/10.1029/2023JG007715, Wiley Online Library on [21/07/2024]. See the Terms and Conditions (https://onlinelibrary.wiley.com/doi/10.1029/2023JG007715, Wiley Online Library on [21/07/2024]. See the Terms and Conditions (https://onlinelibrary.wiley.com/doi/10.1029/2023JG007715, Wiley Online Library on [21/07/2024]. See the Terms and Conditions (https://onlinelibrary.wiley.com/doi/10.1029/2023JG007715, Wiley Online Library on [21/07/2024]. See the Terms and Conditions (https://onlinelibrary.wiley.com/doi/10.1029/2023JG007715, Wiley Online Library on [21/07/2024]. See the Terms and Conditions (https://onlinelibrary.wiley.com/doi/10.1029/2023JG007715, Wiley Online Library on [21/07/2024]. See the Terms and Conditions (https://onlinelibrary.wiley.com/doi/10.1029/2023JG007715, Wiley Online Library on [21/07/2024]. See the Terms and Conditions (https://onlinelibrary.wiley.com/doi/10.1029/2023JG007715, Wiley Online Library on [21/07/2024]. See the Terms and Conditions (https://onlinelibrary.wiley.com/doi/10.1029/2023JG007715, Wiley Online Library on [21/07/2024]. See the Terms and Conditions (https://onlinelibrary.wiley.com/doi/10.1029/2023JG007715, Wiley Online Library on [21/07/2024]. See the Terms and Conditions (https://onlinelibrary.wiley.com/doi/10.1029/2023JG007715, Wiley Online Library on [21/07/2024]. See the Terms and Conditions (https://onlinelibrary.wiley.com/doi/10.1029/2023JG007715, Wiley Online Library on [21/07/2024]. See the Terms and Conditions (https://onlinelibrary.wiley.com/doi/10.1029/2023JG007715, Wiley Online Library on [21/07/2024]. See the Terms and Conditions (https://onlinelibrary.wiley.com/doi/10.1029/2023JG007715, Wiley Online Library.wiley.com/doi/10.1029/2023JG007715, Wiley Online Library.wiley.com/doi/10.1029/2023JG007715, Wiley Online Library.wiley.com/doi/10.1029/2023JG007715, Wiley Onlin

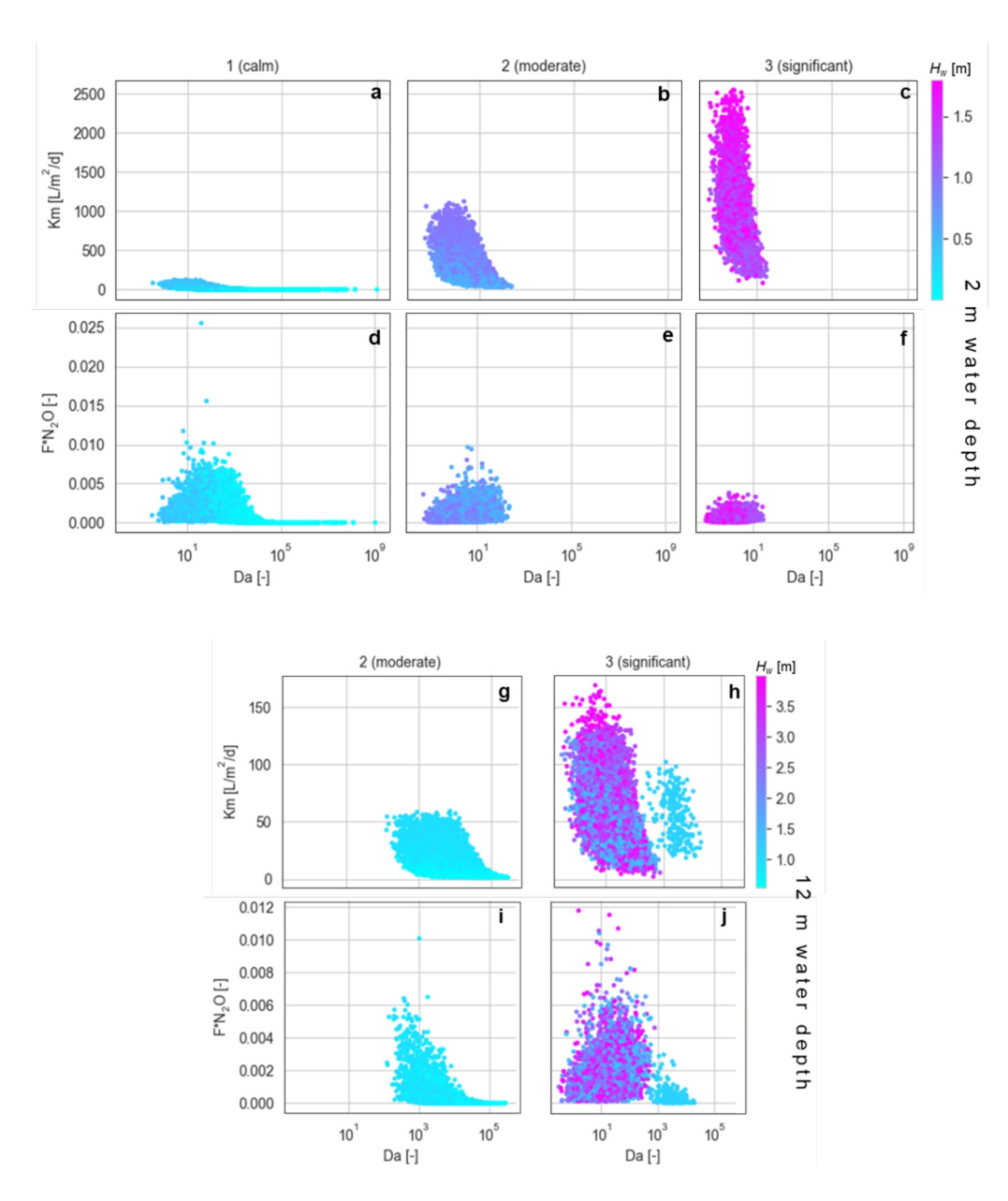


Figure 3. Dependence of pore water exchange (km) and $F*N_2O$ on the Damkohler Number, **Da** (the ratio of time scales for transport and respiration of sediment organic matter) in 2 m (a-f) and 12 m (g-j) water during Monte Carlo simulations.

sediment regulate N_2O efflux. Physical factors explain roughly 60% of the variability in N_2O efflux (with H_w explaining 50% of the variability). DIN_O and nitrification and denitrification fractions (f_{ni} and f_{dn}) are the most influential biogeochemical parameters affecting N_2O efflux (explaining approximately 10% and 30% of the variation during the most intense waves respectively), with an increase in each of these parameters causing a corresponding increase in N_2O efflux (Figure S7 in Supporting Information S1).

 N_2O production was found to depend, to a certain extent, on the Damköhler Number, **Da**, that is, the ratio of time scales for recirculation of solutes through the sediments (which depends on the pore-water exchange rate) and respiration of sediment organic matter (Figure 3). **Da** was mostly greater than 1 in simulations (>85%), indicating that oxygen consumption in the sediment bed is generally transport controlled (the timescale for complete deoxygenation was typically 20 min). The exceptions are events with $H_w > 1$ m in 2 m waters, where transport rates are often higher and oxygen consumptions are often lower. In continental shelf sands, a large fraction of denitrification has been found to be directly linked to oxygen consumption and degradable organic matter supply

FOWDAR ET AL.

21698961, 2024, 7, Downloaded from https://agupubs.on/inlibitary.wiley.com/doi/10.1029/2023JG007715, Wiley Online Library on [21/07/2024]. See the Terms and Conditions (https://onlinelibrary.wiley.com/terms-and-conditions) on Wiley Online Library for rules of use; OA articless of the Terms and Conditions (https://onlinelibrary.wiley.com/terms-and-conditions) on Wiley Online Library for rules of use; OA articless of use of the Terms and Conditions (https://onlinelibrary.wiley.com/terms-and-conditions) on Wiley Online Library for rules of use; OA articless of use of the terms and Conditions (https://onlinelibrary.wiley.com/terms-and-conditions) on Wiley Online Library for rules of use; OA articless of use of

to the sediment (Huettel et al., 2014) which could explain N_2O produced from denitrification. In general, (a) $F*N_2O\approx 0$ (and hence N_2O efflux ≈ 0) at $\mathbf{Da}>10^5$, which correspond to very long residence times, mainly due to a low pore-water exchange rate (wave events with $H_w<0.2$ m (2 m depth) and $H_w<1$ m (12 m depth) fall in this category); (b) At low \mathbf{Da} (<1), $F*N_2O$ is low due to high pore-water exchange rates and limited residence times, respiration rates, nitrification and denitrification, however, N_2O efflux can be high as it is dependent on the porewater exchange rate (a range of wave events fall in this category); (c) At $10 < \mathbf{Da} < 100$, $F*N_2O$ can reach a maximum depending on biogeochemical factors and N_2O efflux depends on both $F*N_2O$ and the pore-water exchange rate (a range of wave events fall in this category).

A direct comparison of the N_2O fluxes in permeable sediments with other coastal systems is complicated by the extremely large range of values modeled here. The vast majority of modeled fluxes were <100 μ mol/m²/d (Figure S6 in Supporting Information S1) and under calm conditions which predominate, the flux of N_2O will typically be < 1 μ mol/m²/d. For comparison, Wong et al. (2013), observed fluxes of ~80 μ mol/m²/d from the nearby eutrophic Werribee Estuary and 200 μ mol/m²/d were observed in the heavily polluted Schelde Estuary (de Wilde & de Bie, 2000). Based on our results here, it is therefore most likely that the fluxes of nitrous oxide from permeable sediments are relatively low compared to eutrophic systems, although spikes of nitrous oxide are likely during periods of high porewater exchange. Further work is required to understand the dynamics of nitrous oxide emissions in response to changing porewater exchange.

4. Conclusions

Our findings suggest that the synergistic effects of increasing eutrophication (e.g., from coastal wastewater disposal practices) and intense hydrodynamic forcing (from high intensity waves) can increase the production of N_2O from biologically active coastal sediments. In particular, we highlight the importance of transport processes, such as wave-induced pore water exchange, in driving benthic N_2O fluxes in coastal settings. Less than 0.5% of seawater DIN flux through the sediment is converted to N_2O , depending on wave climate and water depths. Hence, in addition to seawater DIN concentrations and the emission factors, the rate of the hydrodynamic forcing should be considered in the estimation of the N_2O budget from coastal waters, particularly considring that climate change is expected to cause more severe wave climates. Additionally, our results indicate that even in eutrophic settings such as Werribee, it is highly probable that N_2O emissions as a result of seawater recirculation through permeable sediments is a minor component of total coastal N_2O emissions. For instance, N_2O production was found to occur only during the most intense waves which occur approximately 3% of the time during a year. It is most likely that discharges from groundwater and wastewater treatment plants are more important sources of N_2O emissions in this environment.

Data Availability Statement

Data used in this manuscript as well as the wave data used in the simulations can be found at https://www.hydroshare.org/resource/98104bc112544bd183cb970183cbfbaa/.

References

APHA. (2005). Standard methods for the examination of water and wastewater. American Public Health Association, American Water Works Association, and Water Environment Federation.

Azizian, M., Grant, S. B., Kessler, A. J., Cook, P. L., Rippy, M. A., & Stewardson, M. J. (2015). Bedforms as biocatalytic filters: A pumping and streamline segregation model for nitrate removal in permeable sediments. *Environmental Science & Technology*, 49(18), 10993–11002. https://doi.org/10.1021/acs.est.5b01941

Bange, H. W. (2006). Nitrous oxide and methane in European coastal waters. Estuarine, Coastal and Shelf Science, 70(3), 361–374. https://doi.org/10.1016/j.ecss.2006.05.042

Bardini, L., Boano, F., Cardenas, M. B., Revelli, R., & Ridolfi, L. (2012). Nutrient cycling in bedform induced hyporheic zones. *Geochimica et Cosmochimica Acta*, 84, 47–61. https://doi.org/10.1016/j.gca.2012.01.025

Beaulieu, J. J., Tank, J. L., Hamilton, S. K., Wollheim, W. M., Hall Jr, R. O., Mulholland, P. J., et al. (2011). Nitrous oxide emission from denitrification in stream and river networks. *Proceedings of the National Academy of Sciences*, 108(1), 214–219. https://doi.org/10.1073/pnas. 1011464108

Cardenas, M. B., Cook, P. L. M., Jiang, H. S., & Traykovski, P. (2008). Constraining denitrification in permeable wave-influenced marine sediment using linked hydrodynamic and biogeochemical modeling. *Earth and Planetary Science Letters*, 275(1–2), 127–137. https://doi.org/10.1016/j.epsl.2008.08.016

Chua, E. J., Huettel, M., Fennel, K., & Fulweiler, R. W. (2022). A case for addressing the unresolved role of permeable shelf sediments in ocean denitrification. *Limnology and Oceanography Letters*, 7(1), 11–25. https://doi.org/10.1002/lol2.10218

Ciais, P., Sabine, C., Bala, G., Bopp, L., Brovkin, V., Canadell, J., et al. (2013). Carbon and other biogeochemical cycles. Cambridge.

Acknowledgments

This work was funded by Australian Research Council Grant DP210101595. We would like to acknowledge the assistance of Vera Eate and Sophie Golding Chan for lab measurements. We thank Edoardo Daly and Ravin Deo for support with COMSOL software. Open access publishing facilitated by Monash University, as part of the Wiley - Monash University agreement via the Council of Australian University Librarians.

FOWDAR ET AL. 12 of 14

- Cook, P. L., Wenzhöfer, F., Rysgaard, S., Galaktionov, O. S., Meysman, F. J., Eyre, B. D., et al. (2006). Quantification of denitrification in permeable sediments: Insights from a two-dimensional simulation analysis and experimental data. *Limnology and Oceanography: Methods*, 4(9), 294–307. https://doi.org/10.4319/lom.2006.4.294
- de Wilde, H. P. J., & de Bie, M. J. M. (2000). Nitrous oxide in the Schelde estuary: Production by nitrification and emission to the atmosphere. *Marine Chemistry*, 69(3), 203–216. https://doi.org/10.1016/S0304-4203(99)00106-1
- Elliott, A. H., & Brooks, N. H. (1997). Transfer of nonsorbing solutes to a streambed with bed forms: Theory. Water Resources Research, 33(1), 123–136. https://doi.org/10.1029/96wr02784
- Evrard, V., Glud, R. N., & Cook, P. L. (2013). The kinetics of denitrification in permeable sediments. *Biogeochemistry*, 113(1–3), 563–572. https://doi.org/10.1007/s10533-012-9789-x
- Fogaren, K. E., Sansone, F. J., & De Carlo, E. H. (2013). Porewater temporal variability in a wave-impacted permeable nearshore sediment. *Marine Chemistry*, 149, 74–84. https://doi.org/10.1016/j.marchem.2012.12.005
- Grant, S. B., Gomez-Velez, J. D., Ghisalberti, M., Guymer, I., Boano, F., Roche, K., & Harvey, J. (2020). A one-dimensional model for turbulent mixing in the benthic biolayer of stream and coastal sediments. *Water Resources Research*, 56(12), e2019WR026822. https://doi.org/10.1029/2019wr026822
- Grant, S. B., Stolzenbach, K., Azizian, M., Stewardson, M. J., Boano, F., & Bardini, L. (2014). First-order contaminant removal in the hyporheic zone of streams: Physical insights from a simple analytical model. *Environmental Science & Technology*, 48(19), 11369–11378. https://doi.org/ 10.1021/es501694k
- Harris, G., Batley, G., Fox, D., Hall, D., Jernakoff, P., Molloy, R., et al. (1996). Port Phillip Bay environmental study final report. CSIRO.
- Hirst, A. J., Longmore, A. R., Ball, D., Cook, P. L. M., & Jenkins, G. P. (2016). Linking nitrogen sources utilised by seagrass in a temperate marine embayment to patterns of seagrass change during drought. *Marine Ecology Progress Series*, 549, 79–88. https://doi.org/10.3354/meps11708
- Huettel, M., Berg, P., & Kostka, J. E. (2014). Benthic exchange and biogeochemical cycling in permeable sediments. Annual Review of Marine Science, 6(1), 23–51. https://doi.org/10.1146/annurev-marine-051413-012706
- Hume, A. C., Berg, P., & McGlathery, K. J. (2011). Dissolved oxygen fluxes and ecosystem metabolism in an eelgrass (Zostera marina) meadow measured with the eddy correlation technique. *Limnology & Oceanography*, 56(1), 86–96. https://doi.org/10.4319/lo.2011.56.1.0086
- IPCC. (2019). Refinement to the 2006 IPCC guidelines for national greenhouse gas inventories. Volume 4: Agriculture, forestry and other land use. Chapter 11: N₂O emissions from managed soils, and CO2 emissions from lime and urea application, 2019.
- Ippen, A. T. (1966). Estuary and coastline hydrodynamics. McGraw-Hill Book Company. IncCatalog Card Number 65-27677, Printed in the United States of America.
- Jameson, B. D., Berg, P., Grundle, D. S., Stevens, C. J., & Juniper, S. K. (2021). Continental margin sediments underlying the NE Pacific oxygen minimum zone are a source of nitrous oxide to the water column. *Limnology and Oceanography Letters*, 6(2), 68–76. https://doi.org/10.1002/ lol2.10174
- Kessler, A. J., Glud, R. N., Cardenas, M. B., & Cook, P. L. M. (2013). Transport zonation limits coupled nitrification-denitrification in permeable sediments. *Environmental Science & Technology*, 47(23), 13404–13411. https://doi.org/10.1021/es403318x
- Kessler, A. J., Glud, R. N., Cardenas, M. B., Larsen, M., Bourke, M., & Cook, P. L. M. (2012). Quantifying denitrification in rippled permeable sands through combined flume experiments and modelling. *Limnology & Oceanography*, 57(4), 1217–1232. https://doi.org/10.4319/lo.2012.
- King, J. N., Mehta, A. J., & Dean, R. G. (2009). Generalized analytical model for benthic water flux forced by surface gravity waves. *Journal of Geophysical Research*, 114(C4). https://doi.org/10.1029/2008jc005116
- Maavara, T., Lauerwald, R., Laruelle, G. G., Akbarzadeh, Z., Bouskill, N. J., Van Cappellen, P., & Regnier, P. (2019). Nitrous oxide emissions from inland waters: Are IPCC estimates too high? *Global Change Biology*, 25(2), 473–488. https://doi.org/10.1111/gcb.14504
- Marchant, H. K., Holtappels, M., Lavik, G., Ahmerkamp, S., Winter, C., & Kuypers, M. M. (2016). Coupled nitrification–denitrification leads to extensive N loss in subtidal permeable sediments. Limnology & Oceanography, 61(3), 1033–1048. https://doi.org/10.1002/no.10271
- Marchant, H. K., Tegetmeyer, H. E., Ahmerkamp, S., Holtappels, M., Lavik, G., Graf, J., et al. (2018). Metabolic specialization of denitrifiers in permeable sediments controls N2O emissions. *Environmental Microbiology*, 20(12), 4486–4502. https://doi.org/10.1111/1462-2920.14385
- Marzadri, A., Dee, M. M., Tonina, D., Bellin, A., & Tank, J. L. (2017). Role of surface and subsurface processes in scaling N₂O emissions along riverine networks. *Proceedings of the National Academy of Sciences*, 114(17), 4330–4335. https://doi.org/10.1073/pnas.1617454114
- Mu, Y., Cheng, A. H. D., Badiey, M., & Bennett, R. (1999). Water wave driven seepage in sediment and parameter inversion based on pore pressure data. *International Journal for Numerical and Analytical Methods in Geomechanics*, 23(13), 1655–1674. https://doi.org/10.1002/(sici) 1096-9853(199911)23:13<1655::aid-nag61>3.0.co;2-d
- Murray, R. H., Erler, D. V., & Eyre, B. D. (2015). Nitrous oxide fluxes in estuarine environments: Response to global change. *Global Change Biology*, 21(9), 3219–3245. https://doi.org/10.1111/gcb.12923
- Nevison, C. D., Lueker, T. J., & Weiss, R. F. (2004). Quantifying the nitrous oxide source from coastal upwelling. *Global Biogeochemical Cycles*, 18(1). https://doi.org/10.1029/2003gb002110
- O'Reilly, C., Santos, I. R., Cyronak, T., McMahon, A., & Maher, D. T. (2015). Nitrous oxide and methane dynamics in a coral reef lagoon driven by pore water exchange: Insights from automated high-frequency observations. *Geophysical Research Letters*, 42(8), 2885–2892. https://doi.org/10.1002/2015gl063126
- Precht, E., Franke, U., Polerecky, L., & Huettel, M. (2004). Oxygen dynamics in permeable sediments with wave-driven pore water exchange. Limnology & Oceanography, 49(3), 693–705. https://doi.org/10.4319/lo.2004.49.3.0693
- Precht, E., & Huettel, M. (2003). Advective pore-water exchange driven by surface gravity waves and its ecological implications. *Limnology & Oceanography*, 48(4), 1674–1684. https://doi.org/10.4319/lo.2003.48.4.1674
- Precht, E., & Huettel, M. (2004). Rapid wave-driven advective pore water exchange in a permeable coastal sediment. *Journal of Sea Research*, 51(2), 93–107. https://doi.org/10.1016/j.seares.2003.07.003
- Reeder, W. J., Quick, A. M., Farrell, T. B., Benner, S. G., Feris, K. P., Marzadri, A., & Tonina, D. (2018). Hyporheic source and sink of nitrous oxide. Water Resources Research, 54(7), 5001–5016. https://doi.org/10.1029/2018wr022564
- Riedl, R. J., Huang, N., & Machan, R. (1972). The subtidal pump: A mechanism of interstitial water exchange by wave action. *Marine Biology*, 13(3), 210–221. https://doi.org/10.1007/bf00391379
- Rodellas, V., Cook, P. G., McCallum, J., Andrisoa, A., Meulé, S., & Stieglitz, T. C. (2020). Temporal variations in porewater fluxes to a coastal lagoon driven by wind waves and changes in lagoon water depths. *Journal of Hydrology*, 581, 124363. https://doi.org/10.1016/j.jhydrol.2019.
- Russoniello, C. J., Heiss, J. W., & Michael, H. A. (2018). Variability in benthic exchange rate, depth, and residence time beneath a shallow coastal estuary. *Journal of Geophysical Research: Oceans*, 123(3), 1860–1876. https://doi.org/10.1002/2017jc013568

FOWDAR ET AL. 13 of 14

- Schutte, C. A., Joye, S. B., Wilson, A. M., Evans, T., Moore, W. S., & Casciotti, K. (2015). Intense nitrogen cycling in permeable intertidal sediment revealed by a nitrous oxide hot spot. *Global Biogeochemical Cycles*, 29(10), 1584–1598. https://doi.org/10.1002/2014gb005052
- Seitzinger, S. P. (1988). Denitrification in freshwater and coastal marine ecosystems: Ecological and geochemical significance. *Limnology & Oceanography*, 33(4 part 2), 702–724. https://doi.org/10.4319/lo.1988.33.4part2.0702
- Seitzinger, S. P., & Kroeze, C. (1998). Global distribution of nitrous oxide production and N inputs in freshwater and coastal marine ecosystems. Global Biogeochemical Cycles, 12(1), 93–113. https://doi.org/10.1029/97gb03657
- Shum, K. T. (1993). The effects of wave-induced pore water circulation on the transport of reactive solutes below a rippled sediment bed. *Journal of Geophysical Research*, 98(C6), 10289–10301. https://doi.org/10.1029/93jc00787
- Tian, H., Xu, R., Canadell, J. G., Thompson, R. L., Winiwarter, W., Suntharalingam, P., et al. (2020). A comprehensive quantification of global nitrous oxide sources and sinks. *Nature*, 586(7828), 248–256. https://doi.org/10.1038/s41586-020-2780-0
- Turner, P. A., Griffis, T. J., Baker, J. M., Lee, X., Crawford, J. T., Loken, L. C., & Venterea, R. T. (2016). Regional-scale controls on dissolved nitrous oxide in the Upper Mississippi River. Geophysical Research Letters, 43(9), 4400–4407. https://doi.org/10.1002/2016gl068710
- Warner, J. C., Sherwood, C. R., Signell, R. P., Harris, C. K., & Arango, H. G. (2008). Development of a three-dimensional, regional, coupled wave, current, and sediment-transport model. *Computers & Geosciences*, 34(10), 1284–1306. https://doi.org/10.1016/j.cageo.2008.02.012
- Weiss, R. F., & Price, B. A. (1980). Nitrous oxide solubility in water and seawater. *Marine Chemistry*, 8(4), 347–359. https://doi.org/10.1016/0304-4203(80)90024-9
- Wiberg, P. L., & Harris, C. K. (1994). Ripple geometry in wave-dominated environments. *Journal of Geophysical Research*, 99(C1), 775–789. https://doi.org/10.1029/93jc02726
- Wong, W. W., Cartwright, I., Poh, S. C., & Cook, P. (2022). Sources and cycling of nitrogen revealed by stable isotopes in a highly populated large temperate coastal embayment. Science of the Total Environment, 806, 150408. https://doi.org/10.1016/j.scitotenv.2021.150408
- Wong, W. W., Grace, M. R., Cartwright, I. C., Cardenas, M. B., Zamora, P. B., & Cook, P. L. M. (2013). Dynamics of groundwater-derived nitrate and nitrous oxide in a tidal estuary from radon mass balance modeling. *Limnology & Oceanography*, 58(5), 1689–1706. https://doi.org/10.4319/lo.2013.58.5.1689
- Wong, W. W., Greening, C., Shelley, G., Lappan, R., Leung, P. M., Kessler, A., et al. (2021). Effects of drift algae accumulation and nitrate loading on nitrogen cycling in a eutrophic coastal sediment. *Science of the Total Environment*, 790, 147749. https://doi.org/10.1016/j.scitotenv. 2021.147749
- Yang, S., Chang, B. X., Warner, M. J., Weber, T. S., Bourbonnais, A. M., Santoro, A. E., et al. (2020). Global reconstruction reduces the uncertainty of oceanic nitrous oxide emissions and reveals a vigorous seasonal cycle. *Proceedings of the National Academy of Sciences*, 117(22), 11954–11960. https://doi.org/10.1073/pnas.1921914117

FOWDAR ET AL. 14 of 14